LETTER
SPACE PHYSICS: MAGNETOSPHERIC PHYSICS

Earth and Planetary Physics
3: 365–372, 2019
doi: 10.26464/epp2019037

Ring current proton scattering by low-frequency magnetosonic waves

Jiang Yu[1], Jing Wang[1*], and Jun Cui[1,2,3]

[1]Space Science Institute, Macau University of Science and Technology, Macau, China;

[2]School of Atmospheric Sciences, Sun Yat-sen University, Zhuhai Guangdong 519082, China;

[3]Key Laboratory of Lunar and Deep Space Exploration, Chinese Academy of Sciences, Beijing 100012, China

Abstract: Magnetosonic (MS) waves are believed to have the ability to affect the dynamics of ring current protons both inside and outside the plasmasphere. However, previous studies have focused primarily on the effect of high-frequency MS waves (f > 20 Hz) on ring current protons. In this study, we investigate interactions between ring current protons and low-frequency MS waves (< 20 Hz) inside the plasmasphere. We find that low-frequency MS waves can effectively accelerate < 20 keV ring current protons on time scales from several hours to a day, and their scattering efficiency is comparable to that due to high-frequency MS waves (>20 Hz), from which we infer that omitting the effect of low-frequency MS waves will considerably underestimate proton depletion at middle pitch angles and proton enhancement at large pitch angles. Therefore, ring current proton modeling should take into account the effects of both low- and high-frequency MS waves.

Keywords: magnetosonic waves; ring current protons; wave-particle interactions; proton distribution evolutions

Citation: Yu, J., Wang, J., and Cui, J. (2019). Ring current proton scattering by low-frequency magnetosonic waves. *Earth Planet. Phys.*, *3*(4), 365–372. http://doi.org/10.26464/epp2019037

1. Introduction

Magnetosonic (MS) waves, also known as equatorial noise, are predominantly observed near the magnetic equator at frequencies between the proton cyclotron frequency (f_{cp}) and the lower hybrid resonance frequency (f_{LHR}) both inside and outside the plasmasphere (Russell et al., 1970; Perraut et al., 1982; Santolík et al., 2002; Meredith et al., 2008; Fu HS et al., 2014; Posch et al., 2015; Li LY et al., 2017a, b; Yuan ZG et al., 2017; Liu X et al., 2018; Liu B et al., 2018). These waves are mostly linearly polarized; they propagate nearly perpendicular to the background magnetic field (Zhima et al., 2015; Yu J et al., 2017; Su ZP et al., 2017), and they are believed to be excited by proton ring distributions (Horne et al., 2000; Chen LJ et al., 2010, 2011; Liu KJ et al., 2011; Xiao FL et al., 2013). Recently, MS waves have caught much attention because, by resonating with particles, they play a crucial role in radiation belt dynamics. On the one hand, numerous studies have found that these emissions are able to produce electron butterfly distributions via Landau resonance and bounce resonance energization (Horne et al., 2007; Shprits, 2009; Bortnik and Thorne, 2010; Li JX et al., 2014; Li LY et al., 2017a; Ni BB et al., 2017, 2018; Tao X and Li X, 2016; Xiao FL et al., 2015). On the other hand, MS waves are also found capable of interacting with protons through cyclotron resonance (Xiao FL et al., 2014; Fu S et al., 2016). However, the interaction between MS waves and protons has drawn much less attention. Based on quasi-linear theory, Xiao FL et al. (2014) proposed that MS wave-induced proton precipitation is a potential mechanism accounting for the proton aurora. Recently, the test particle simulations by Fu S et al. (2016) indicated that MS waves have the ability to accelerate ring current protons both inside and outside the plasmasphere.

The ring current ions consist primarily of H^+, He^+, and O^+ ions with energies from 1 keV up to hundreds of keV in the inner magnetosphere, from $2R_E$ to $9R_E$ (e.g., Daglis et al., 1999; Ebihara and Miyoshi, 2011). Some observations and simulations have demonstrated that MS wave-induced pitch angle and energy diffusion are able to contribute significantly to the dynamics of ring current protons (e.g. Xiao FL et al., 2014; Fu S et al., 2016). Previous studies have concentrated mainly on effects of high-frequency MS waves (f >20 Hz) on ring current protons; effects of low-frequency (f <20 Hz) MS waves on ring current ions have so far been lacking, despite the fact that low-frequency MS waves have commonly been observed in the magnetosphere, especially in the high-density plasmasphere (Perraut et al., 1982; Posch et al., 2015).

In this paper, we investigate interactions between ring current protons and a representative low-frequency MS waves event, detected on 21 August 2013. By performing 2-D Fokker-Planck simulations, we further examine the effect of low-frequency MS waves on the pitch angle distribution evolution of ring current protons.

2. Observations of Low-Frequency MS Waves

Figure 1 shows a representative event of strong low-frequency MS waves, measured by the Electric and Magnetic Field Instrument

Correspondence to: J. Wang, wangjingjlu@hotmail.com
Received 18 APR 2019; Accepted 10 MAY 2019.
Accepted article online 28 MAY 2019.

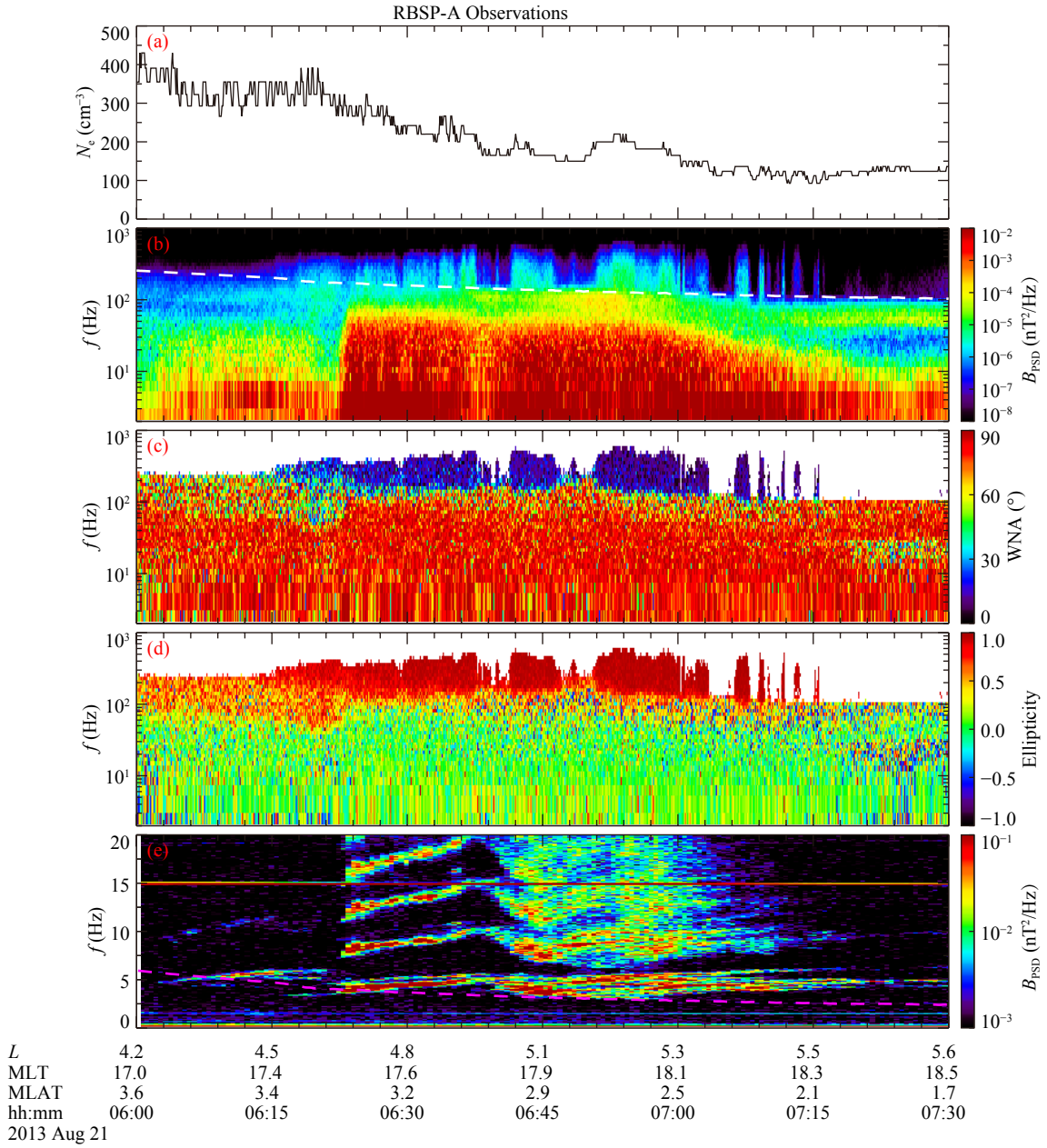

Figure 1. An overview of the intense MS wave event inside the plasmasphere on 21 August 2013. (a) Plasma density. (b, e) Power spectral density of magnetic field. (c) Wave normal angle. (d) Polarization ellipticity. The white and pink dashed curves denote the lower hybrid resonance frequency and the proton gyrofrequency.

Suite and Integrated Science (EMFISIS) instrument (Kletzing et al., 2013) onboard the Radiation Belt Storm Probe A (RBSP-A) near the duskside magnetic equator (MLT~18 h and MLAT < 3°) between 06:00 and 07:30 UT on 21 August 2013. As shown in Figure 1a, the plasma density inferred from the upper hybrid resonance frequency (Kurth et al., 2015) is larger than 100 cm^{-3}, indicating that the RBSP-A satellite was inside the plasmasphere during this period of interest. When inside the plasmasphere, the satellite observes intense emissions, with frequencies extending down to local proton gyrofrequency between 06:22 and 07:10 UT. Before 06:40 UT, these emissions clearly exhibit harmonic structures, and thereafter evolve gradually into broadband emissions. The wave normal angle (WNA) and polarization ellipticity (Figures 1c–1d) derived from the singular value decomposition (SVD) method (Santolík et al., 2003) indicate that these emissions are nearly perpendicularly propagating and linearly polarized. These wave properties confirm that the amplified emissions are magnetosonic waves (Yu J et al., 2017).

3. Proton Scattering Rates

Figures 2a and 2b show the power spectral density of waves in the frequency ranges from 0 to 20 Hz and from 20 to 80 Hz between 06:40 and 06:50 UT at L ~5.2. Green dots and the red curve represent the measurements and the mean value of power spectral density, respectively. Three peaks, around 4, 9 and 12 Hz, are found in the MS wave power spectral density. Above 12 Hz, the wave intensity fluctuates slightly and decreases gradually, from

~2×10^{-2} nT^2/Hz at 12 Hz to ~4×10^{-5} nT^2/Hz at 80 Hz.

The resonance condition between MS waves and protons is described as:

$$\omega - kv\cos\alpha\left(1+X^2\right)^{-1/2} = n\Omega_p/\gamma, \quad (1)$$

where ω is wave frequency, k is the wave number, v is the proton velocity, α is the local pitch angle, X is the tangent of wave normal angle, n is the resonance order, Ω_p is the proton gyrofrequency, and γ is the Lorentz factor. For given resonance orders and wave frequencies, the minimum resonant energy of protons can be calculated through combination of the resonance condition and the cold plasma dispersion relation. The cold plasma dispersion relation is given by Stix (1962):

$$D(k,\omega,X) = \left(SX^2+P\right)\mu^4 - \left(RLX^2+PS\left(2+X^2\right)\right)\mu^2 + PRL\left(1+X^2\right) = 0, \quad (2)$$

where $\mu = kc/\omega$ is the refractive index, c is the speed of light, and R, L, S, P are the usual Stix coefficients (Stix, 1962).

Figures 2c and 2d show the minimum resonant energy of protons as a function of resonance order and wave frequency for WNA = 88.6° and WNA = 89°, using the measured background magnetic field strength (B = 208 nT) and plasma density (N_e = 167 cm^{-3}), respectively. Ring current protons can resonate with MS waves (f < 80 Hz) when the resonance order is smaller than 30. The higher frequency MS waves can interact with ring current protons through higher order cyclotron resonance. Additionally, the resonant frequency range of MS waves interacting with ring current protons narrows for a given resonance order when MS waves propagate more perpendicular to the background magnetic field (larger WNAs).

To analyze the scattering efficiency of ring current protons quantitatively, we assume that MS waves are confined within MLAT < 3°, and both the MS wave spectral intensity and the background plasma density remain constant along the magnetic field lines. According to previous studies (e.g. Horne et al., 2007; Yu J et al., 2019), the tangent of the wave normal angle (X = tan θ) is assumed to be a Gaussian distribution

$$g(x) = \exp\left[-\left(\frac{X-X_m}{X_w}\right)^2\right],\ X_{min} < X < X_{max}$$

with peak at X_m = tan 89°, half-width X_w = tan 86°, and lower and upper cutoffs $X_{min} = X_m - X_w$ and $X_{max} = X_m + X_w$. Following previous studies (Lyons, 1974; Glauert and Horne, 2005), the bounce-averaged diffusion coefficients in a dipole field can be written as:

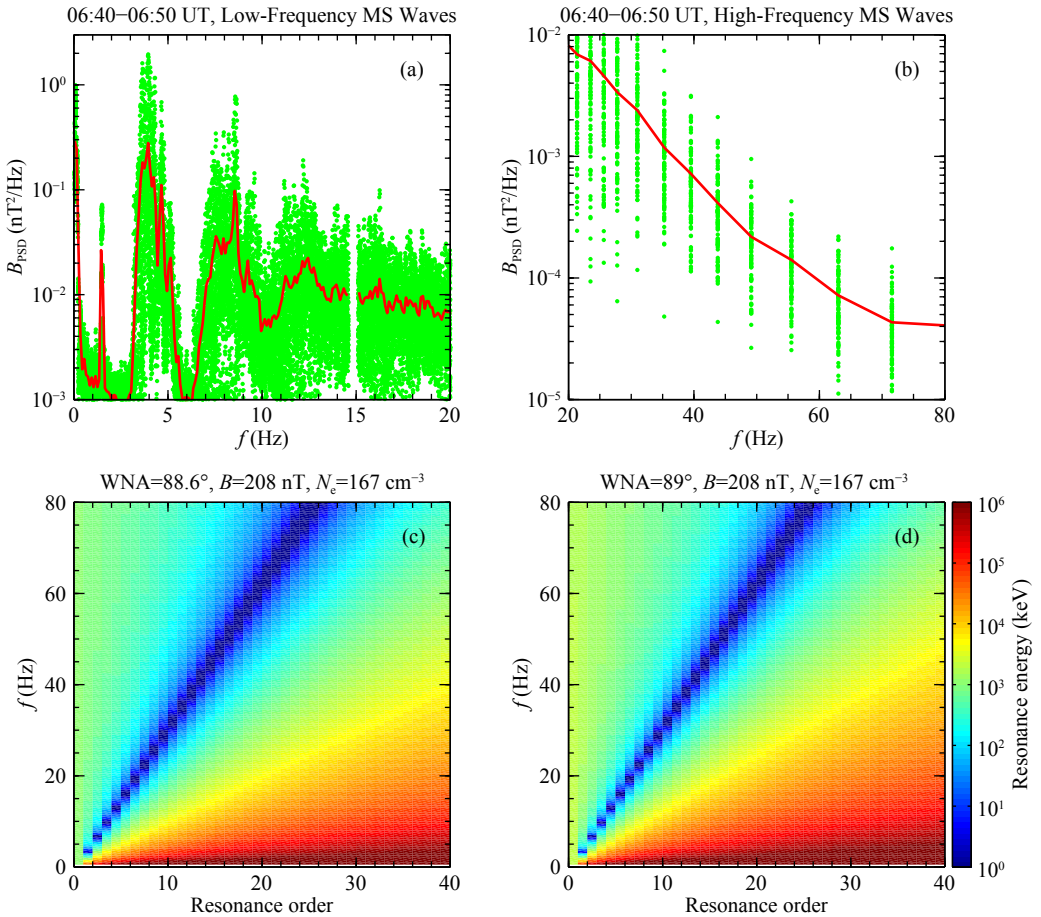

Figure 2. (a, b) Power spectral density of low-frequency and high-frequency MS waves. (c-d) Resonance energy as a function of resonance order and wave frequency for WNA = 88.6° and WNA = 89°. Green dots and red curve represent measurements and the mean value of power spectral density.

$$\langle D_{\alpha\alpha}\rangle = \frac{1}{T(\alpha_{\rm eq})}\int_0^{\lambda_{\rm m}} D_{\alpha\alpha}\frac{\cos\alpha}{\cos^2\alpha_{\rm eq}}\cos^7\lambda {\rm d}\lambda, \tag{3}$$

$$\langle D_{\alpha p}\rangle = \frac{1}{T(\alpha_{\rm eq})}\int_0^{\lambda_{\rm m}} D_{\alpha p}\frac{\cos^4\lambda(1+3\cos^2\lambda)^{1/4}}{\cos\alpha_{\rm eq}}{\rm d}\lambda, \tag{4}$$

$$\langle D_{pp}\rangle = \frac{1}{T(\alpha_{\rm eq})}\int_0^{\lambda_{\rm m}} D_{pp}\frac{\cos\lambda(1+3\cos^2\lambda)^{1/2}}{\cos\alpha}{\rm d}\lambda, \tag{5}$$

where $T(\alpha_{\rm eq}) = 1.30 - 0.56\sin\alpha_{\rm eq}$, $\alpha_{\rm eq}$ is the equatorial pitch angle, $\lambda_{\rm m}$ is the mirror latitude, $D_{\alpha\alpha}$, $D_{\alpha p}$, D_{pp} are local pitch angle, cross, and momentum diffusion coefficients, which are written as:

$$D_{\alpha\alpha} = \sum_{n=n_l}^{n_h}\int_{X_{\rm min}}^{X_{\rm max}} X{\rm d}X D_{\alpha\alpha}^{nX}, \tag{6}$$

$$D_{\alpha p} = \sum_{n=n_l}^{n_h}\int_{X_{\rm min}}^{X_{\rm max}} X{\rm d}X D_{\alpha p}^{nX}, \tag{7}$$

$$D_{pp} = \sum_{n=n_l}^{n_h}\int_{X_{\rm min}}^{X_{\rm max}} X{\rm d}X D_{pp}^{nX}, \tag{8}$$

with

$$D_{\alpha\alpha}^{nX} = \sum_i \frac{e^2\omega_i^2}{4\pi(1+X^2)N(\omega_i)}\left[\frac{n\Omega_{\rm p}/(\gamma\omega_i)-\sin^2\alpha}{\cos\alpha}\right]^2 \times B^2(\omega_i)\,g(X)\,\frac{\left|\Phi_{n,k}\right|^2}{\left|v\cos\alpha - \sqrt{1+X^2}\dfrac{\partial\omega}{\partial k}\right|}\Bigg|_{k_i}, \tag{9}$$

$$D_{\alpha p}^{nX} = D_{\alpha\alpha}^{nX}\left[\frac{\sin\alpha\cos\alpha}{n\Omega_{\rm p}/(\gamma\omega_i)-\sin^2\alpha}\right]_{k_i}, \tag{10}$$

$$D_{pp}^{nX} = D_{\alpha\alpha}^{nX}\left[\frac{\sin\alpha\cos\alpha}{n\Omega_{\rm p}/(\gamma\omega_i)-\sin^2\alpha}\right]_{k_i}^2. \tag{11}$$

The local diffusion coefficients are evaluated at the resonant frequency ω_i and the resonant wave number k_i which satisfy the resonant condition (equation (1)) and the dispersion relation for MS waves (equation (2)). $B^2(\omega_i)$ is the wave power spectral density. The term $\left|\Phi_{n,k}\right|^2$ is associated with the wave refractive index and $N(\omega_i)$ is a normalization factor (see Lyons, 1974; Glauert and Horne, 2005).

In our calculations, the bounce-averaged diffusion coefficients of ring current protons are evaluated by including contributions from harmonic resonances up to n = ±15 for low-frequency MS waves and n = ±40 for high-frequency MS waves. Figure 3 shows the bounce-averaged pitch angle ($<D_{\alpha\alpha}>/p^2$), momentum ($<D_{pp}>/p^2$), and cross ($|<D_{\alpha p}>|/p^2$) diffusion coefficients of ring current protons driven by low-frequency and high-frequency MS waves. Clearly, the diffusion coefficients are very small near the loss cone ($\alpha_{\rm LC}$ ~4°, $<D_{\alpha\alpha}/p^2>$ ~10^{-9} s^{-1}). The momentum diffusion coefficients of protons are much larger than the pitch angle diffusion coefficients at larger pitch angles and higher energies, indicating that MS waves mainly accelerate ring current protons rather than precipitate them into the atmosphere. For 1–10 keV protons, the large momentum diffusion coefficients ($<D_{pp}/p^2>$ ~10^{-5}–10^{-4} s^{-1}) suggest that MS waves can accelerate these protons on time scales from several hours to a day. The diffusion coefficients driv-

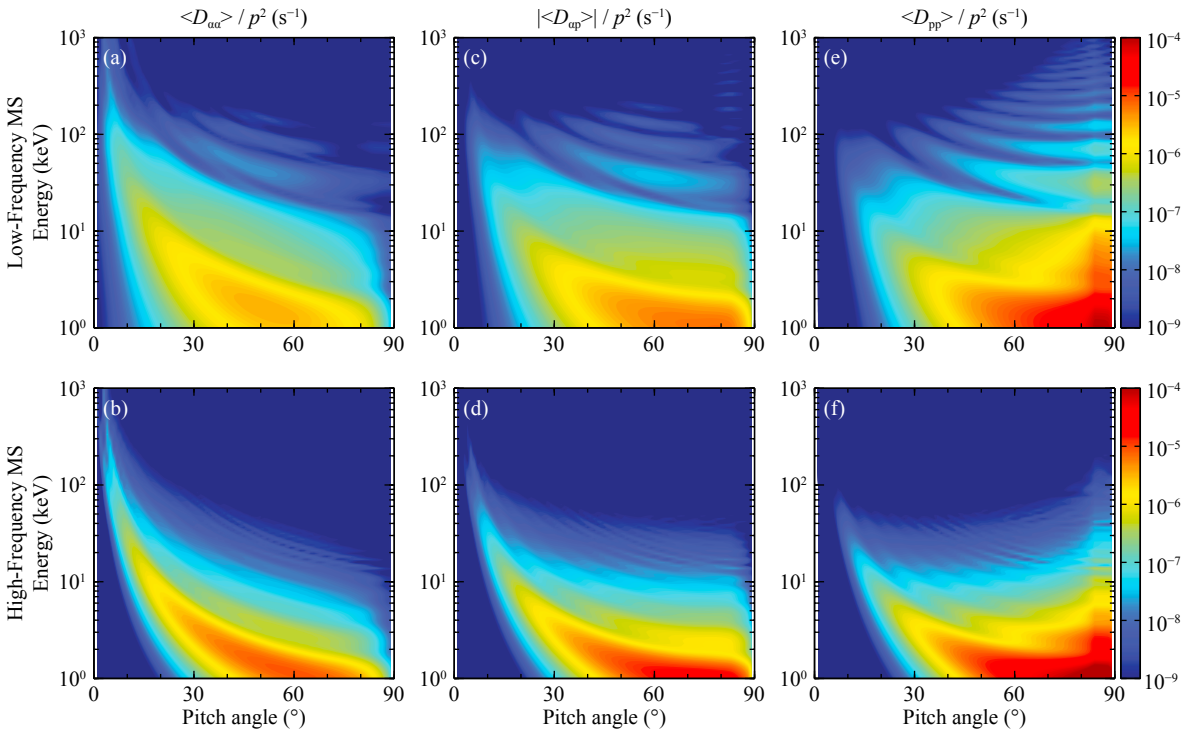

Figure 3. Pitch angle diffusion coefficients, cross diffusion coefficients, and energy diffusion coefficients driven by low-frequency (top) and high-frequency (bottom) MS waves.

en by low-frequency MS waves are comparable to those by high-frequency MS waves. Therefore, the effect of low-frequency MS waves on ring current protons is significant.

Using 2-D Fokker-Planck diffusion equations, we simulate the temporal evolution of proton distributions due to different-frequency MS waves. The initial pitch angle (α_{eq}) distribution of ring current protons is assumed to be a function of $\sin(\alpha_{eq})$. The boundary conditions of the normalized proton phase space density (PSD) are written as: $F = 0$ at $\alpha_{eq} = \alpha_{LC}$ (α_{LC} is the loss cone), $\partial F/\partial \alpha_{eq} = 0$ at $\alpha_{eq} = 90°$, F = constant at $E = 1$ keV and $F = 0$ at $E = 1$ MeV. Figure 4 shows the proton temporal evolution scattered by low-frequency MS waves only, high-frequency MS waves only, and combined diffusion, at the indicated times. Low-energy protons (<20 keV) are efficiently scattered by both low-frequency and high-frequency MS waves, whereas high-energy protons (>20 keV) are not strongly affected. For low-energy protons, the scattering efficiency due to low-frequency MS waves is comparable to that due to high-frequency MS waves. However, the PSD enhancement of near-equatorially mirroring protons in the energy range 10–20 keV driven by low-frequency MS waves is stronger than that by high-frequency MS waves (Figures 4j and 4k). The <10 keV protons at middle pitch angles (e.g. $30° < \alpha_{eq} < 60°$) are scattered more efficiently by higher-frequency MS waves. Combining the effects of low-frequency and high-frequency MS waves, the scattering of low-energy protons is seen to be more pronounced at middle pitch angles.

Figure 5 shows the line plots of proton temporal evolution driven by low-frequency MS waves only (left), high-frequency MS waves only (middle), and combined scattering (right) at different proton energies. Both low- and high-frequency MS waves can scatter 2 and 5 keV protons at almost all pitch angles. However, for 10 and 20 keV protons, the MS wave-driven energization is effective only at small and large pitch angles. For higher energy protons (10 and 20 keV), the acceleration caused by lower-frequency MS waves is more pronounced. Additionally, for 2 and 10 keV protons, the combined scattering leads to a stronger proton depletion at middle pitch angles and a stronger proton enhancement at large pitch angles. Overall, the MS waves cause proton temperature anisotropyto increase.

4. Conclusions and Discussions

In this study, we present a representative event of low-frequency MS waves observed by Radiation Belt Storm Probe A near the duskside magnetic equator (MLT ~18 h and MLAT < 3°) inside the plasmasphere on 21 August 2013. The wave power of MS waves is concentrated mainly below 20 Hz, and the lowest emission frequency extends down to the local proton gyrofrequency (~ 3 Hz). We analyze the wave-particle interactions between ring current protons and low-frequency MS waves (< 20 Hz) by performing 2-D Fokker-Planck diffusion simulations based on the data from this event. The numerical results show that low-frequency MS waves can effectively accelerate < 20 keV ring current protons on time

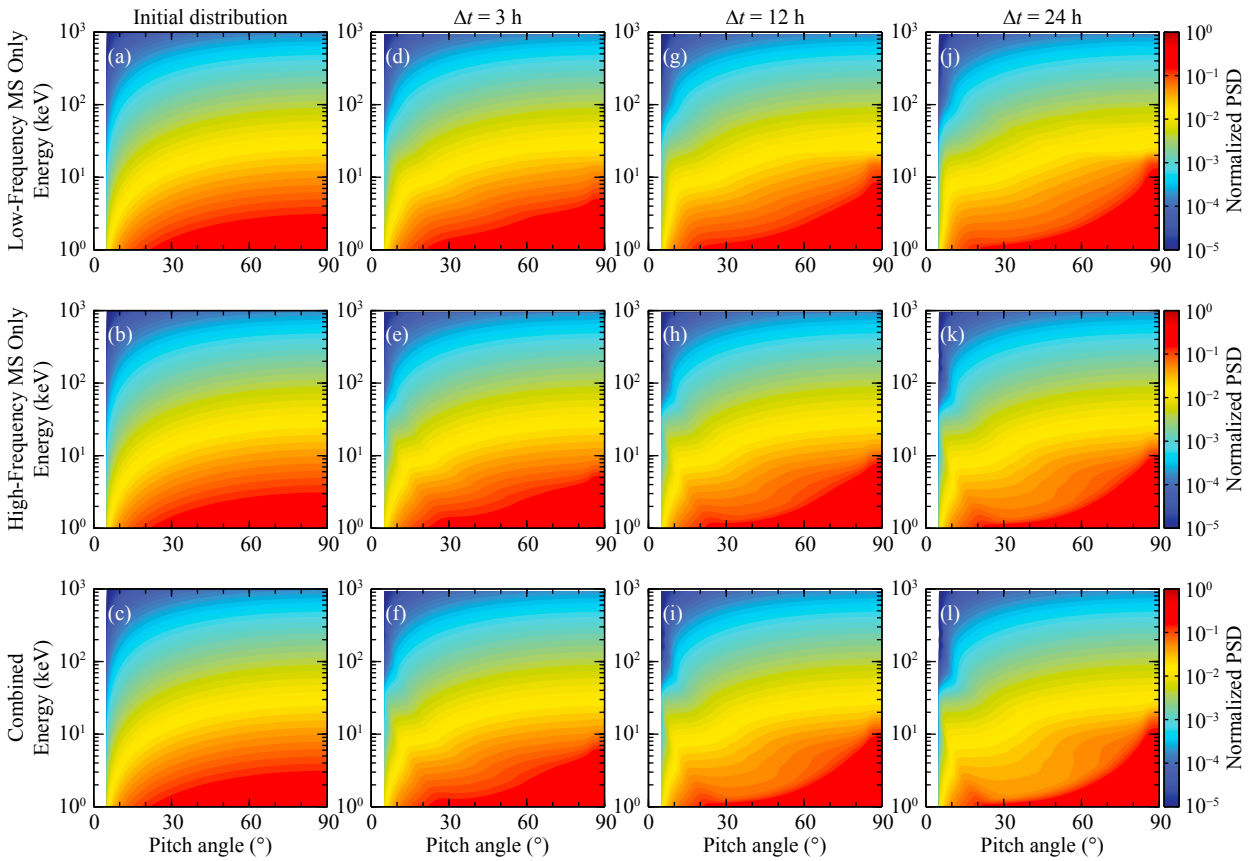

Figure 4. The proton temporal evolution scattered by low-frequency MS waves only (top), high-frequency MS waves only (middle), and combined diffusion (bottom), at different indicated times.

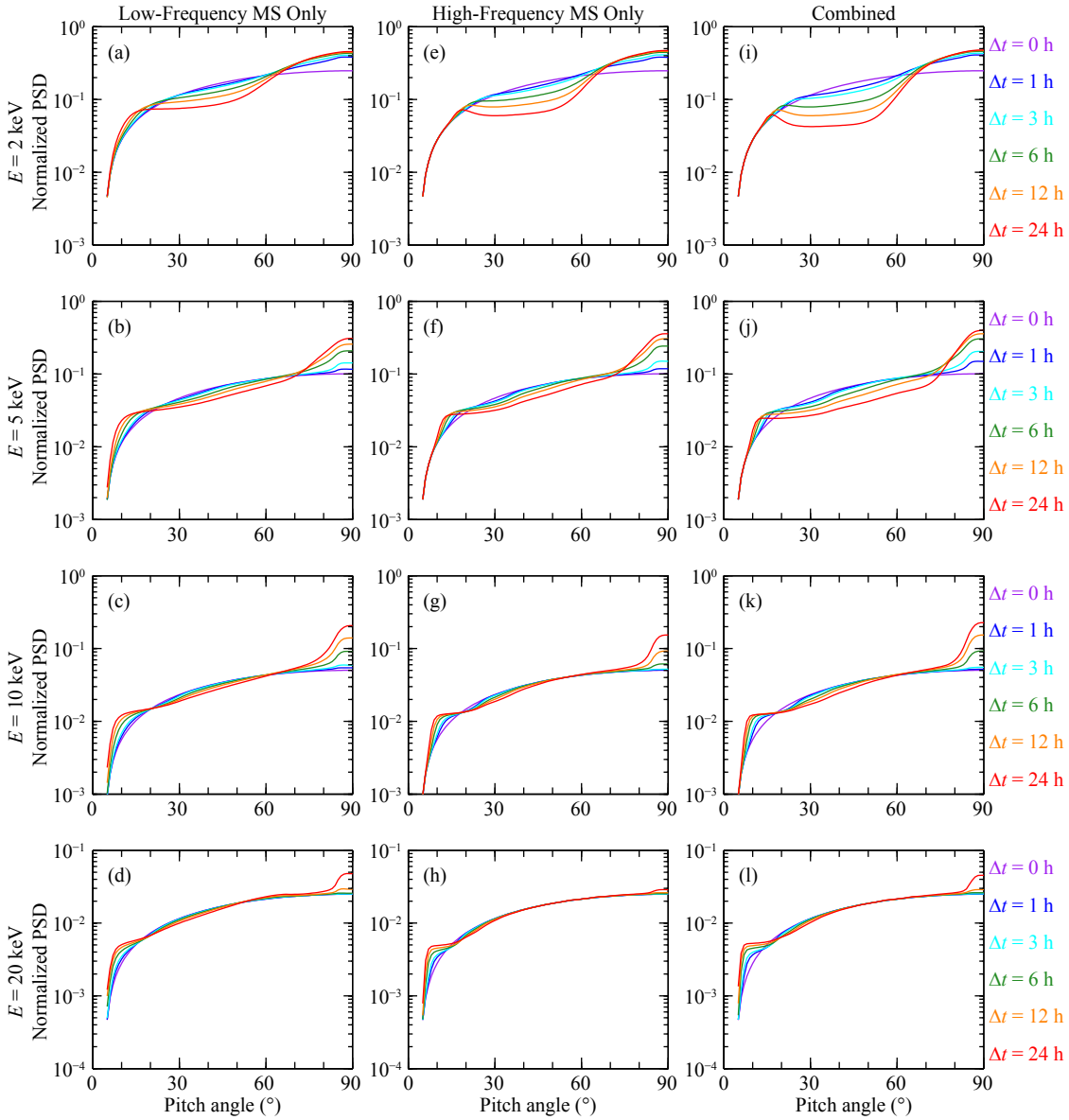

Figure 5. The line plots of proton temporal evolution driven by low-frequency MS waves only (left), high-frequency MS waves only (middle), and combined scattering (right), at different proton energies. Different color lines denote the proton phase space densities at different interaction times.

scales from several hours to a day, and their scattering efficiency is comparable to that due to high-frequency MS waves (>20 Hz).

Omitting the effect of low-frequency MS waves will considerably underestimate proton depletion at middle pitch angles and proton enhancement at large pitch angles. The proton enhancement observed in the quasi-perpendicular direction suggests that low-frequency MS waves can cause significant temperature anisotropy of ring current protons. The temperature anisotropy of keV protons can further excite electromagnetic ion cyclotron (EMIC) waves (Cao JB et al., 1995, 1998a, b; Chen LJ et al., 2010; Wang ZQ et al., 2017a). Intense EMIC waves lead to rapid precipitation loss of relativistic electrons and ring current protons through cyclotron resonance (Yuan ZG et al., 2010; Usanova et al., 2014; Ni BB et al., 2015; Yu J et al., 2015; Li LY et al., 2016; Cao X et al., 2016; Wang ZQ et al., 2017b, c). Therefore, low- and high-frequency MS waves appear jointly to influence the dynamics of both ring current protons and radiation belt electrons.

Acknowledgments

Jiang Yu and Jun Cui are supported by the Science and Technology Development Fund of Macau SAR (FDCT) through grants 039/2013/A2. The authors also acknowledge supports from the National Natural Science Foundation of China (NSFC) through grants 41525015 and 41774186. RBSP data are available at https://emfisis.physics.uiowa.edu/data/index.

References

Bortnik, J., and Thorne, R. M. (2010). Transit time scattering of energetic electrons due to equatorially confined magnetosonic waves. *J. Geophys. Res. Space Phys.*, *115*(A7), A07213. https://doi.org/10.1029/2010JA015283

Cao, J. B., Mazelle, C., Belmont, G., and Rème, H. (1995). Nongyrotropy of heavy newborn ions at comet Grigg-Skjellerup and corresponding instability. *J. Geophys. Res. Space Phys.*, *100*(A12), 23379–23388. https://doi.org/10.1029/95JA01915

Cao, J. B., Zhou, G. C., and Wang, X. Y. (1998a). Generalized ion ring instability driven by ions with a partial shell distribution. *Geophys. Res. Lett.*, *25*(9), 1499–1501. https://doi.org/10.1029/98GL01006

Cao, J. B., Mazelle, C., Belmont, G., and Rème, H. (1998b). Oblique ring instability driven by nongyrotropic ions: application to observations at comet Grigg-Skjellerup. *J. Geophys. Res. Space Phys.*, *103*(A2), 2055–2067. https://doi.org/10.1029/97JA02370

Cao, X., Ni, B. B., Liang, J., Xiang, Z., Wang, Q., Shi, R., Gu, X. D., Zhou, C., Zhao, Z. Y., ... Liu, J. (2016). Resonant scattering of central plasma sheet protons by multiband emic waves and resultant proton loss timescales. *J. Geophys. Res. Space Phys.*, *121*(2), 1219–1232. https://doi.org/10.1002/2015JA021933

Chen, L. J., Thorne, R. M., Jordanova, V. K., and Horne, R. B. (2010). Global simulation of magnetosonic wave instability in the storm time magnetosphere. *J. Geophys. Res. Space Phys.*, *115*(A11), A11222. https://doi.org/10.1029/2010JA015707

Chen, L. J., Thorne, R. M., Jordanova, V. K., Thomsen, M. F., and Horne, R. B. (2011). Magnetosonic wave instability analysis for proton ring distributions observed by the LANL magnetospheric plasma analyzer. *J. Geophys. Res. Space Phys.*, *116*(A3), A03223. https://doi.org/10.1029/2010JA016068

Daglis, I. A., Thorne, R. M., Baumjohann, W., and Orsini, S. (1999). The terrestrial ring current: origin, formation, and decay. *Rev. Geophys.*, *37*(4), 407–438. https://doi.org/10.1029/1999RG900009

Ebihara, Y., and Miyoshi, Y. (2011). Dynamic inner magnetosphere: a tutorial and recent advances, In W. Liu (Ed.), *The Dynamic Magnetosphere* (Vol. 3, pp. 145-187). Dordrecht: Springer. https://doi.org/10.1007/978-94-007-0501-2_9

Fu, H. S., Cao, J. B., Zhima, Z., Khotyaintsev, Y. V., Angelopoulos, V., Santolík, O., Omura, Y., Taubenschuss, U., Chen, L., and Huang, S. Y. (2014). First observation of rising-tone magnetosonic waves. *Geophys. Res. Lett.*, *41*(21), 7419–7426. https://doi.org/10.1002/2014GL061867

Fu, S., Ni, B. B., Li, J. X., Zhou, C., Gu, X. D., Huang, S. Y., Zhang, H., Ge, Y. S., and Cao X. (2016). Interactions between magnetosonic waves and ring current protons: gyroaveraged test particle simulations. *J. Geophys. Res. Space Phys.*, *121*(9), 8537–8553. https://doi.org/10.1002/2016JA023117

Glauert, S. A., and Horne, R. B. (2005). Calculation of pitch angle and energy diffusion coefficients with the PADIE code. *J. Geophys. Res. Space Phys.*, *110*(A4), A04206. https://doi.org/10.1029/2004JA010851

Horne, R. B., Wheeler, G. V., and Alleyne, H. S. C. K. (2000). Proton and electron heating by radially propagating fast magnetosonic waves. *J. Geophys. Res. Space Phys.*, *105*(A12), 27597–27610. https://doi.org/10.1029/2000JA000018

Horne, R. B., Thorne, R. M., Glauert, S. A., Meredith, N. P., Pokhotelov, D., and Santolík, O. (2007). Electron acceleration in the van Allen radiation belts by fast magnetosonic waves. *Geophys. Res. Lett.*, *34*(17), L17107. https://doi.org/10.1029/2007GL030267

Kletzing, C. A., Kurth, W. S., Acuna, M., MacDowall, R. J., Torbert, R. B., Averkamp, T., Bodet, D., Bounds, S. R., Chutter, M., … Tyler, J. (2013). The electric and magnetic field instrument suite and integrated science (EMFISIS) on RBSP. *Space Sci. Rev.*, *179*(1-4), 127–181. https://doi.org/10.1007/s11214-013-9993-6

Kurth, W. S., De Pascuale, S., Faden, J. B., Kletzing, C. A., Hospodarsky, G. B., Thaller, S., and Wygant, J. R. (2015). Electron densities inferred from plasma wave spectra obtained by the waves instrument on Van Allen Probes. *J. Geophys. Res. Space Phys.*, *120*(2), 904–914. https://doi.org/10.1002/2014JA020857

Li, J. X., Ni, B. B., Xie, L., Pu, Z. Y., Bortnik, J., Thorne, R. M., Chen, L. J., Ma, Q. L., Fu, S. Y., … Guo, R. L. (2014). Interactions between magnetosonic waves and radiation belt electrons: comparisons of quasi-linear calculations with test particle simulations. *Geophys. Res. Lett.*, *41*(14), 4828–4834. https://doi.org/10.1002/2014GL060461

Li, L. Y., Yu, J., Cao, J. B., and Yuan, Z. G. (2016). Compression-amplified emic waves and their effects on relativistic electrons. *Phys. Plasmas*, *23*(6), 062116. https://doi.org/10.1063/1.4953899

Li, L. Y., Yu, J., Cao, J. B., Yang, J. Y., Li, X., Baker, D. N., Reeves, G. D., and Spence, H. (2017a). Roles of whistler mode waves and magnetosonic waves in changing the outer radiation belt and the slot region. *J. Geophys. Res. Space Phys.*, *122*(5), 5431–5448. https://doi.org/10.1002/2016JA023634

Li, L. Y., Liu, B., Yu, J., and Cao, J. B. (2017b). The rapid responses of magnetosonic waves to the compression and expansion of Earth's magnetosphere. *Geophys. Res. Lett.*, *44*(22), 11239–11247. https://doi.org/10.1002/2017GL075649

Liu, B., Li, L. Y., Yu, J., and Cao, J. B. (2018). The effect of hot protons on magnetosonic waves inside and outside the plasmapause: new observations and theoretic results. *J. Geophys. Res. Space Phys.*, *123*(1), 653–664. https://doi.org/10.1002/2017JA024676

Liu, K. J., Gary, S. P., and Winske, D. (2011). Excitation of magnetosonic waves in the terrestrial magnetosphere: particle-in-cell simulations. *J. Geophys. Res. Space Phys.*, *116*(A7), A07212. https://doi.org/10.1029/2010JA016372

Liu, X., Chen, L. J., Yang, L. X., Xia, Z. Y., and Malaspina, D. M. (2018). One-dimensional full wave simulation of equatorial magnetosonic wave propagation in an inhomogeneous magnetosphere. *J. Geophys. Res. Space Phys.*, *123*(1), 587–599. https://doi.org/10.1002/2017JA024336

Lyons, L. R. (1974). Pitch angle and energy diffusion coefficients from resonant interactions with ion-cyclotron and whistler waves. *J. Plasma Phys.*, *12*(3), 417–432. https://doi.org/10.1017/S002237780002537X

Meredith, N. P., Horne, R. B., and Anderson, R. R. (2008). Survey of magnetosonic waves and proton ring distributions in the Earth's inner magnetosphere. *J. Geophys. Res. Space Phys.*, *113*(A6), A06213. https://doi.org/10.1029/2007JA012975

Ni, B. B., Cao, X., Zou, Z. Y., Zhou, C., Gu, X. D., Bortnik, J., Zhang, J. C., Fu, S., Zhao, Z. Y., … Xie, L. (2015). Resonant scattering of outer zone relativistic electrons by multiband emic waves and resultant electron loss time scales. *J. Geophys. Res. Space Phys.*, *120*(9), 7357–7373. https://doi.org/10.1002/2015JA021466

Ni, B. B., Hua, M., Zhou, R. X., Yi, J., and Fu, S. (2017). Competition between outer zone electron scattering by plasmaspheric hiss and magnetosonic waves. *Geophys. Res. Lett.*, *44*(8), 3465–3474. https://doi.org/10.1002/2017GL072989

Ni, B. B., Zou, Z. Y., Fu, S., Cao, X., Gu, X. D., and Xiang, Z. (2018). Resonant scattering of radiation belt electrons by off-equatorial magnetosonic waves. *Geophys. Res. Lett.*, *45*(3), 1228–1236. https://doi.org/10.1002/2017GL075788

Perraut, S., Roux, A., Robert, P., Gendrin, R., Sauvaud, J. A., Bosqued, J. M., Kremser, G., and Korth, A. (1982). A systematic study of ULF waves above F_{H+} from GEOS 1 and 2 measurements and their relationships with proton ring distributions. *J. Geophys. Res. Space Phys.*, *87*(A8), 6219–6236. https://doi.org/10.1029/JA087iA08p06219

Posch, J. L., Engebretson, M. J., Olson, C. N., Thaller, S. A., Breneman, A. W., Wygant, J. R., Boardsen, S. A., Kletzing, C. A., Smith, C. W., and Reeves, G. D. (2015). Low-harmonic magnetosonic waves observed by the Van Allen Probes. *J. Geophys. Res. Space Phys.*, *120*(8), 6230–6257. https://doi.org/10.1002/2015JA021179

Russell, C. T., Holzer, R. E., and Smith, E. J. (1970). OGO 3 observations of ELF noise in the magnetosphere: 2. The nature of the equatorial noise. *J. Geophys. Res.*, *75*(4), 755–768. https://doi.org/10.1029/JA075i004p00755

Santolík, O., Pickett, J. S., Gurnett, D. A., Maksimovic, M., and Cornilleau-Wehrlin, N. (2002). Spatiotemporal variability and propagation of equatorial noise observed by Cluster. *J. Geophys. Res. Space Phys.*, *107*(A12), 1495. https://doi.org/10.1029/2001JA009159

Santolík, O., Parrot, M., and Lefeuvre, F. (2003). Singular value decomposition methods for wave propagation analysis. *Radio Sci.*, *38*(1), 1010. https://doi.org/10.1029/2000RS002523

Shprits, Y. Y. (2009). Potential waves for pitch-angle scattering of near-equatorially mirroring energetic electrons due to the violation of the second adiabatic invariant. *Geophys. Res. Lett.*, *36*(12), L12106. https://doi.org/10.1029/2009GL038322

Stix, T. H. (1962). *The Theory of Plasma Waves*. New York: McGraw-Hill.

Su, Z. P., Wang, G., Liu, N. G., Zheng, H. N., Wang, Y. M., and Wang, S. (2017). Direct observation of generation and propagation of magnetosonic waves following substorm injection. *Geophys. Res. Lett.*, *44*(15), 7587–7597. https://doi.org/10.1002/2017GL074362

Tao, X., and Li, X. (2016). Theoretical bounce resonance diffusion coefficient for waves generated near the equatorial plane. *Geophys. Res. Lett.*, *43*(14), 7389–7397. https://doi.org/10.1002/2016GL070139

Usanova, M. E., Drozdov, A., Orlova, K., Mann, I. R., Shprits, Y., Robertson, M. T., Turner, D. L., Milling, D. K., Kale, A., … Wygant, J. (2014). Effect of EMIC waves on relativistic and ultrarelativistic electron populations: ground-based and Van Allen Probes observations. *Geophys. Res. Lett.*, *41*(5), 1375–1381. https://doi.org/10.1002/2013GL059024

Wang, Z.Q., Zhai, H., Gao, Z. X., and Huang, C. Y. (2017a). Gyrophase bunched ions in the plasma sheet. *Adv. Space Res.*, *59*(1), 274–282. https://doi.org/10.1016/j.asr.2016.08.003

Wang, Z. Q., Pan, Z. R., Zhai, H., Gao, Z. X., Sun, K., & Zhang, Y. S. (2017b). The nonlinear interactions between O^+ ions and oxygen band EMIC waves. *J. Geophys. Res. Space Phys.*, *122*(7), 7097–7109. https://doi.org/10.1002/2017JA024113

Wang, Z. Q., Zhai, H., and Gao, Z. X. (2017c). The effects of hydrogen band EMIC waves on ring current H^+ ions. *Geophys. Res. Lett.*, *44*(23), 11722–11728. https://doi.org/10.1002/2017GL075843

Xiao, F. L., Zhou, Q. H., He, Z. G., Yang, C., He, Y. H., and Tang, L. J. (2013). Magnetosonic wave instability by proton ring distributions: simultaneous data and modeling. *J. Geophys. Res. Space Phys.*, *118*(7), 4053–4058. https://doi.org/10.1002/jgra.50401

Xiao, F. L., Zong, Q. G., Wang, Y. F., He, Z. G., Su, Z. P., Yang, C., and Zhou, Q. H. (2014). Generation of proton aurora by magnetosonic waves. *Sci. Rep.*, *4*, 5190. https://doi.org/10.1038/srep05190

Xiao, F. L., Yang, C., Su, Z. P., Zhou, Q. H., He, Z. G., He, Y. H., Baker, D. N., Spence, H. E., Funsten, H. O., and Blake, J. B. (2015). Wave-driven butterfly distribution of Van Allen belt relativistic electrons. *Nat. Commun.*, *6*, 8590. https://doi.org/10.1038/ncomms9590

Yu, J., Li, L. Y., Cao, J. B., Yuan, Z. G., Reeves, G. D., Baker, D. N., Blake, J. B., and Spence, H. (2015). Multiple loss processes of relativistic electrons outside the heart of outer radiation belt during a storm sudden commencement. *J. Geophys. Res. Space Phys.*, *120*(12), 10275–10288. https://doi.org/10.1002/2015JA021460

Yu, J., Li, L. Y., Cao, J. B., Chen, L., Wang, J., and Yang, J. (2017). Propagation characteristics of plasmaspheric hiss: Van Allen Probe observations and global empirical models. *J. Geophys. Res. Space Phys.*, *122*(4), 4156–4167. https://doi.org/10.1002/2016JA023372

Yu, J., Li, L. Y., Cui, J., Cao J. B., and Wang, J. (2019). Effect of low-harmonic magnetosonic waves on the radiation belt electrons inside the Plasmasphere. *J. Geophys. Res. Space Phys.*. https://doi.org/10.1029/2018JA026328

Yuan, Z. G., Deng, X. H., Lin, X., Pang, Y., Zhou, M., Décréau, P. M. E., Trotignon, J. G., Lucek, E., Frey, H. U., and Wang, J. F. (2010). Link between EMIC waves in a plasmaspheric plume and a detached sub-auroral proton arc with observations of Cluster and IMAGE satellites. *Geophys. Res. Lett.*, *37*(7), L07108. https://doi.org/10.1029/2010GL042711

Yuan, Z. G., Yu, X. D., Huang, S. Y., Wang, D. D., and Funsten, H. O. (2017). In situ observations of magnetosonic waves modulated by background plasma density. *Geophys. Res. Lett.*, *44*(15), 7628–7633. https://doi.org/10.1002/2017GL074681

Zhima, Z., Chen, L. J., Fu, H. S., Cao, J. B., Horne, R. B., and Reeves, G. (2015). Observations of discrete magnetosonic waves off the magnetic equator. *Geophys. Res. Lett.*, *42*(22), 9694–9701. https://doi.org/10.1002/2015GL066255